

# Self-consistent autocorrelation for finite-area bias correction in roughness measurement

D Nečas

CEITEC, Brno University of Technology, Purkyňova 123, 61200 Brno, Czech Republic

E-mail: [yeti@gwyddion.net](mailto:yeti@gwyddion.net)

**Abstract.** Scan line levelling, a ubiquitous and often necessary step in AFM data processing, can cause a severe bias on measured roughness parameters such as mean square roughness or correlation length. This work exploits the observation that the bias of autocorrelation function (ACF) is expressed in terms of the function itself, permitting a self-consistent formulation of the problem. Using this formulation, two correction approaches are proposed, both with the aim to obtain convenient formulae which can be applied to practical correction. The first modifies standard analytical models of ACF to incorporate, in expectation, the bias and thus match the bias of the data the models are used to fit. The second inverts the relation between true and estimated ACF to realise a model-free correction.

*Keywords:* Scanning Probe Microscopy, roughness, autocorrelation, bias

## 1. Introduction

Recently a couple of works drew attention to how roughness measurement by atomic force microscopy (AFM) are impacted by levelling/background subtraction [1, 2], in particular line levelling, a ubiquitous and often necessary step in AFM data processing [3–6]. The classic results for the effect of mean value subtraction on statistical quantities [7–9] were generalised in a theoretical framework covering many common levelling methods. The mean square roughness  $\sigma$ , as well as many other quantities, becomes biased. For 1D data and 1D scan line levelling the bias of estimate  $\hat{\sigma}$  can be written (in expectation):

$$\mathbb{E}[\hat{\sigma}^2] = \sigma^2 - 2 \int_0^1 G(tL) C(t) dt . \quad (1)$$

Function  $G$  is the true autocorrelation function (ACF) of the roughness and  $C$  a complicated function capturing correlation/spectral properties of the specific levelling method. Explicit expressions for the second term—measurement bias—are known for several common levelling methods and autocorrelation function forms. [1] It should be noted that is more correct to call  $G$  the autocovariance function and reserve the

term autocorrelation for the function normalised to variance, but both are commonly used. The bias problem is not unique to AFM and profilometry data levelling. Similar problems occur for autocovariance function estimation from locally smoothed (detrended) data [10, 11].

Ultimately, the bias and variance depend on the ratio  $\alpha = T/L$  of correlation length  $T$  and scan line length  $L$  and the bias increases with ‘aggressivity’ of the levelling procedure [1, 8]. The ratio  $\alpha$  must be kept small for reliable results. If scan line levelling and similar 1D corrections are applied the error is proportional to  $\alpha$  (not  $\alpha^2$  as one might assume for 2D image data), which can be difficult to keep sufficiently small. Even when scan lines are not levelled explicitly, the computation of 1D ACF imposes the condition of mean zero value on image rows, corresponding to degree-0 polynomial levelling. The length  $L$  is, unfortunately, also often not set deliberately but instead to what ‘feels right’ [2]. This then translates to  $\alpha$  which is way too large—sometimes far beyond instrumental constraints. Bias estimation procedures, nevertheless, exist, either simple and coarse [2] or more detailed [1], allowing one to check whether it is within reasonable bounds.

All the bias estimates are based on knowing the correlation length  $T$ . However, the value estimated from data  $\hat{T}$  is itself biased (underestimated) because the ACF is affected in a similar manner as  $\sigma^2$ , as illustrated in figure 1. Furthermore, assumptions about the form of ACF are also generally necessary. This creates an chicken and egg problem. Therefore, although the estimates help with assessing the impact on a particular measurement, they are of limited use for obtaining unbiased (bias-corrected) values of basic roughness parameters such as  $\sigma$  and  $T$ , or of the ACF. A convenient bias correction method is still missing. This work aims to provide the missing piece. It is sought in the form of a simple yet effective augmentation of existing computations in order to enable wide adoption.

The overall plan is fairly straightforward. We begin from the observation that the value of ACF at zero is  $\sigma^2$ , that is  $\sigma^2 = G(0)$ . Formula (1) can thus be also written

$$\mathbb{E}[\hat{G}(0)] = G(0) - 2 \int_0^1 G(tL) C(t) dt . \quad (2)$$

The second (bias) term is linear in  $G$ . Imagine an expression of the same form can be obtained for  $G$  as a whole (we show later that it is indeed the case)

$$\mathbb{E}[\hat{G}] = G - RG . \quad (3)$$

Here  $R$  is a linear operator expressing the bias, now of the entire ACF. It again captures the properties of the specific levelling procedure. Expression (3) ties self-consistently together the true and estimated ACF. We can say that the ACF knows about its own bias. The relation can be formally inverted to

$$G = (1 - R)^{-1} \mathbb{E}[\hat{G}] , \quad (4)$$

yielding unbiased  $G$  from the biased estimate  $\hat{G}$  (in expectation). This is the adventurous option.

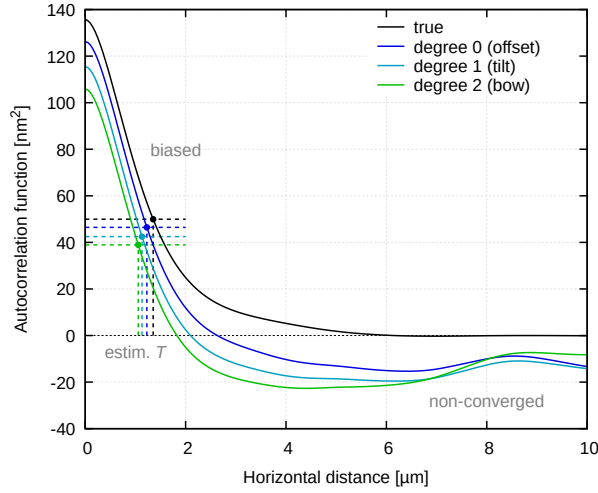


**Figure 1.** The effect of scan line polynomial levelling using polynomials of various degrees on the estimated ACF. The beginning of the curve (small distances) is biased, whereas for larger distances the ACF estimate is not converged and exhibits oscillations [8].

The conservative option is to employ expression (3) directly. Assume, for instance, that the roughness is Gaussian. The true ACF has then the form

$$G_{\text{Gauss}}(\tau) = \sigma^2 \exp\left(-\frac{\tau^2}{T^2}\right). \quad (5)$$

Usually we fit the estimated ACF  $\hat{G}(\tau)$  with this model  $G_{\text{Gauss}}(\tau)$  with  $\sigma$  and  $T$  as free parameters. But it is clearly the wrong model. The correct model is  $G_{\text{Gauss}}(\tau) - R G_{\text{Gauss}}(\tau)$  and it can be obtained by applying  $R$  to  $G_{\text{Gauss}}(\tau)$ .

The questions are whether  $R$  and  $(1 - R)^{-1}$  can be reasonably evaluated and how well the correction will work in practice. They are explored in the following sections. The general expression for  $R$  is derived in section 2, which the reader can skip on the first reading. Section 3 provides elementary formulae and procedures for practical bias correction and section 4 tests their effectiveness using simulations and real AFM data.

## 2. Bias of ACF after levelling

The calculation of  $R$  follows the general scheme and notation introduced in Ref. 1 (sections 3.1 and 3.3), including treating the data as continuous functions. Since 1D (scan line) levelling is the dominant effect even for image data [2], we consider the 1D case. Denote  $\varphi_j$  orthonormal basis functions used for background subtraction by linear fitting, with  $j$  distinguishing the functions. If  $\varphi_j$  are polynomials then  $j \in \{0, 1, 2, \dots, n-1\}$  is the degree, but the index may not be a simple integer in other cases. Summations over  $j$  are, therefore, written below only formally.

Levelled data are computed by subtracting the projection onto the span of  $\varphi_j$

$$\hat{z}(x) = z(x) - \sum_j a_j \varphi_j(x), \quad (6)$$

with coefficients  $a_j$  equal to the dot products

$$a_j = \int_0^L z(x) \varphi_j(x) dx . \quad (7)$$

The ACF is estimated as

$$\hat{G}(\tau) = \frac{1}{L-\tau} \int_0^{L-\tau} \hat{z}(x) \hat{z}(x+\tau) dx . \quad (8)$$

Substituting expressions (6) into (8) gives for  $\hat{G}(\tau)$

$$\frac{1}{L-\tau} \int_0^{L-\tau} \left[ z(x) - \sum_j a_j \varphi_j(x) \right] \left[ z(x+\tau) - \sum_k a_k \varphi_k(x+\tau) \right] dx , \quad (9)$$

which can be expanded into four terms corresponding to the combinations of  $z$  and  $\varphi$ :

$$\hat{G}(\tau) = \hat{G}_1(\tau) - \hat{G}_2(\tau) - \hat{G}_3(\tau) + \hat{G}_4(\tau) . \quad (10)$$

Taking expectations,

$$\begin{aligned} \mathbb{E}[\hat{G}_1(\tau)] &= G(\tau) \\ \mathbb{E}[\hat{G}_2(\tau)] &= \frac{1}{L-\tau} \sum_j \int_0^{L-\tau} \int_0^L G(x' - x + \tau) \varphi_j(x) \varphi_j(x') dx' dx \\ \mathbb{E}[\hat{G}_3(\tau)] &= \frac{1}{L-\tau} \sum_k \int_0^{L-\tau} \int_0^L G(x' - x) \varphi_k(x + \tau) \varphi_j(x') dx' dx \\ \mathbb{E}[\hat{G}_4(\tau)] &= \frac{1}{L-\tau} \sum_{j,k} \left[ \int_0^L \int_0^L G(x'' - x') \varphi_k(x') \varphi_j(x'') dx' dx'' \right. \\ &\quad \left. \times \int_0^{L-\tau} \varphi_j(x) \varphi_k(x + \tau) dx \right] , \end{aligned} \quad (11)$$

where we utilised the linearity of expectation and that for any  $a$  and  $b$

$$\mathbb{E}[z(a)z(b)] = G(b - a) = G(a - b) . \quad (12)$$

In a similar manner as in formula (1) for the bias of  $\sigma^2$ , one term (here  $\mathbb{E}[\hat{G}_1]$ ) gives the unbiased  $G(\tau)$  and the remaining terms combine to give the bias  $RG(\tau)$ .

### 2.1. Linear operator $R$

In principle, formulae (11) can already be considered a representation of the operator  $R$ . However, it is more natural (and useful) to write it explicitly

$$\mathbb{E}[\hat{G}(\tau)] = G(\tau) - \int_0^L R(\tau, u) G(u) du . \quad (13)$$

Meaning in  $E[\hat{G}_2(\tau)]$  we must set  $u = x' - x + \tau$ , transform the domain of integration (which splits the integral into three) and obtain

$$\begin{aligned} E[\hat{G}_2(\tau)] = \frac{1}{L-\tau} \sum_j & \left[ \int_0^{L-\tau} G(u) c_{j,[0,L-\tau-u]}(\tau+u) du \right. \\ & + \int_0^\tau G(u) c_{j,[0,L-\tau]}(\tau-u) du \\ & \left. + \int_\tau^L G(u) c_{j,[u-\tau,L-\tau]}(\tau-u) du \right]. \end{aligned} \quad (14)$$

The symmetry of  $G$  was utilised to ensure its argument is always positive and thus from interval  $[0, L]$ . Functions  $c_j$  again express the correlation properties of  $\varphi_j$ , in analogy to Ref. 1. However, as the various integrals are over different subintervals of  $[0, L]$  they are more complicated here, defined

$$c_{j,[a,b]}(\delta) = \int_a^b \varphi_j(x) \varphi_j(x+\delta) dx. \quad (15)$$

Finally, in order to transform the expression to the form (13), we replace the integration limits for  $u$  using the indicator function

$$\chi_{[a,b]}(x) = \begin{cases} 1 & \text{if } a \leq x \leq b \\ 0 & \text{otherwise} \end{cases} \quad (16)$$

resulting in

$$\begin{aligned} E[\hat{G}_2(\tau)] = \frac{1}{L-\tau} \int_0^L G(u) \sum_j & \left[ \chi_{[0,L-\tau]}(u) c_{j,[0,L-\tau-u]}(\tau+u) \right. \\ & + \chi_{[0,\tau]}(u) c_{j,[0,L-\tau]}(\tau-u) \\ & \left. + \chi_{[\tau,L]}(u) c_{j,[u-\tau,L-\tau]}(\tau-u) \right] du. \end{aligned} \quad (17)$$

The term in square brackets is one piece of  $R(\tau, u)$  in the form required by (13)—the one corresponding to  $\hat{G}_2$ . The second piece, corresponding to  $\hat{G}_3$ , is obtained using the same steps. The last piece contains integrals combining  $\varphi_j$  and  $\varphi_k$  for  $j \neq k$  that cannot be expressed using (15). If we define

$$c_{j,k,b}(\delta) = \int_0^b \varphi_j(x) \varphi_k(x+\delta) dx. \quad (18)$$

it can be written

$$E[\hat{G}_4(\tau)] = \frac{1}{L-\tau} \int_0^L G(u) \sum_{j,k} [c_{j,k,L-u}(u) + c_{k,j,L-u}(u)] c_{j,k,L-\tau}(\tau) du \quad (19)$$

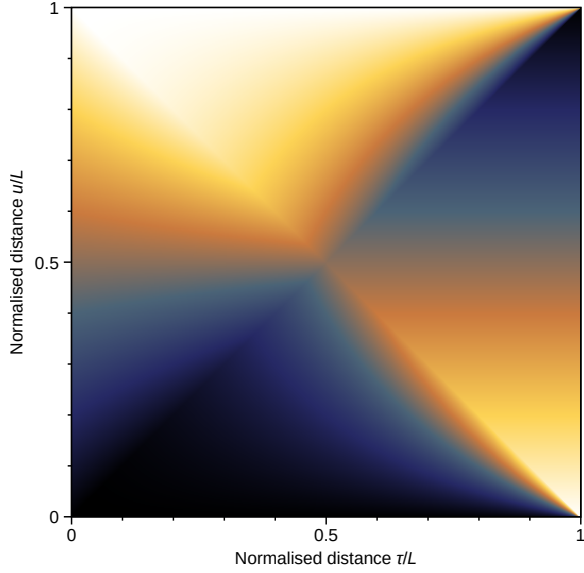


**Figure 2.** Linear operator  $R_0(\tau, u)$  for mean value subtraction, normalised to  $L$  (equivalent to putting  $L = 1$ ). The false colour scale corresponds to the interval  $[0, 2]$ .

Therefore, the final expression for  $R(\tau, u)$  is

$$\begin{aligned}
 R(\tau, u) = & \frac{1}{L - \tau} \sum_j \left[ \chi_{[0, L-\tau]}(u) (c_{j, [0, L-\tau-u]}(\tau + u) + c_{j, [\tau+u, L]}(-\tau - u)) \right. \\
 & + \chi_{[0, \tau]}(u) (c_{j, [0, L-\tau]}(\tau - u) + c_{j, [\tau, L]}(u - \tau)) \\
 & \left. + \chi_{[\tau, L]}(u) (c_{j, [u-\tau, L-\tau]}(\tau - u) + c_{j, [\tau, L+\tau-u]}(u - \tau)) \right] \quad (20) \\
 & - \frac{1}{L - \tau} \sum_{j,k} [c_{j,k, L-u}(u) + c_{k,j, L-u}(u)] c_{j,k, L-\tau}(\tau)
 \end{aligned}$$

## 2.2. Polynomial levelling

A polynomial basis  $\varphi_j$  has symmetries which can be used simplify  $R(\tau, u)$  somewhat. We first note that the expression is unwieldy because  $R(\tau, u)$  is inherently complex, with a number of discontinuities in the derivative. Even for mean value subtraction, when the single basis function  $\varphi_0$  is a constant, we get

$$R_0(\tau, u) = \frac{2}{L} \left[ \chi_{[0, L-\tau]}(u) \frac{L - \tau - u}{L - \tau} + \chi_{[0, \tau]}(u) \frac{u - \tau}{L - \tau} + \frac{(L - u)\tau}{L(L - \tau)} \right], \quad (21)$$

illustrated in figure 2. Although only function values for small  $\tau$  and  $u$  are important and some of the discontinuities can thus be disregarded,  $R(\tau, u)$  is not totally differentiable at  $(0, 0)$ . A small- $\tau$  approximation of the entire integral in (13) is possible only because the integral is a smoother function than  $R(\tau, u)$ .

For general polynomials, we note that Legendre polynomials  $P_n(x)$  on interval  $[-1, 1]$  are either even or odd,  $P_n(-x) = (-1)^n P_n(x)$ . For the orthonormal basis functions on  $[0, L]$  it translates to

$$\varphi_j(L - x) = (-1)^j \varphi_j(x). \quad (22)$$

From this we can easily see that

$$c_{j,k,L-\tau}(\tau) = (-1)^{j+k} c_{k,j,L-\tau}(\tau) . \quad (23)$$

Terms with  $j + k$  odd can be omitted as they mutually cancel. And for  $j + k$  even only terms with  $j < k$  can be kept, multiplied by 2. Together with the relation  $c_{j,j,b} = c_{j,[0,b]}$ , permitting rewriting terms with  $j = k$ , these rules eliminate most of the terms in the second summation in (20). In fact, for degree 1 no such term remains, giving

$$\begin{aligned} R_1(\tau, u) = \frac{1}{L - \tau} \sum_{j=0}^1 & \left[ \chi_{[0,L-\tau]}(u) (c_{j,[0,L-\tau-u]}(\tau + u) + c_{j,[\tau+u,L]}(-\tau - u)) \right. \\ & + \chi_{[0,\tau]}(u) (c_{j,[0,L-\tau]}(\tau - u) + c_{j,[\tau,L]}(u - \tau)) \\ & + \chi_{[\tau,L]}(u) (c_{j,[u-\tau,L-\tau]}(\tau - u) + c_{j,[\tau,L+\tau-u]}(u - \tau)) \\ & \left. - 2c_{j,[0,L-u]}(u) c_{j,[0,L-\tau]}(\tau) \right] \quad (24) \end{aligned}$$

A similar simplification is possible for other bases formed by even and odd functions  $\varphi_j$ , for instance sines and cosines, although the indexing by  $j$  may differ (and sines and cosines are more natural to handle in the frequency domain). However, the small- $(\tau, u)$  expansion for a specific basis is still tedious and better evaluated using symbolic algebra software.

Maxima [12] was used to obtain the practical formulae summarised in the following section. The expansions were terminated at  $\alpha^2$  terms. The first reason is that preliminary numerical experiments showed that the leading  $\alpha^1$  terms is not always sufficient and without the second term there is a tendency to overcorrection. The general form of  $\sigma^2$  bias for polynomial levelling contains only even-power terms after  $\alpha^2$  (equation (27) in Ref. 1). Therefore, there is no  $\alpha^3$  term in the expansion and higher powers are negligible. Finally, the low smoothness of  $R$  at zero means that more accurate expansions would not be, in general, Taylor-like and would have to include more complicated ACF-specific terms.

### 3. Practical formulae

#### 3.1. Corrected models

The (biased) discrete ACF is estimated from data values  $z_k$  [8]

$$\hat{G}_k = \frac{1}{N - k} \sum_{m=0}^{N-1-k} z_m z_{m+k} , \quad (25)$$

where  $\tau = k\Delta_x$  if  $\Delta_x$  is the sampling step. It is fitted by an ACF model function. Simple models have only two free parameters,  $\sigma$  and  $T$ . The classic Gaussian ACF model (5) and analogous exponential model

$$G_{\text{exp}}(\tau) = \sigma^2 \exp\left(-\frac{\tau}{T}\right) . \quad (26)$$

are replaced with the leading terms of  $(G - BG)(\tau)$  expanded for small  $\alpha$  and  $\tau$ . In particular, the Gaussian model is replaced with

$$G_{\text{Gauss}}^{\text{bias}}(\tau) = \sigma^2 \exp\left(-\frac{\tau^2}{T^2}\right) - \sqrt{\pi}n\sigma^2 \frac{T}{L} \left(1 + \frac{\tau}{L}\right) + n^2\sigma^2 \frac{T^2}{L^2} \left(1 + \frac{2\tau}{L}\right) \quad (27)$$

and the exponential model with

$$G_{\text{exp}}^{\text{bias}}(\tau) = \sigma^2 \exp\left(-\frac{\tau}{T}\right) - 2n\sigma^2 \frac{T}{L} \left(1 + \frac{\tau}{L}\right) + 2n^2\sigma^2 \frac{T^2}{L^2} \left(1 + \frac{2\tau}{L}\right) . \quad (28)$$

The superscript <sup>bias</sup> indicates the models are biased, matching the bias of the data (25) they are used to fit. Models (27) and (28) should be fitted from zero to approximately the first zero crossing, i.e. up to the first  $k$  for which  $G_k < 0$ .

The biased models do not have any additional free parameters. Nevertheless, they contain two additional inputs, the profile or scan line length  $L$  and the number of terms  $n$  of the line levelling polynomial—which is one plus its degree. Expressions (27) and (28) can be simplified by introducing ratios  $\alpha = T/L$  and  $t = \tau/L$ , but one must keep in mind  $\alpha$  and  $t$  contain the free fitting parameter  $T$  and the independent variable  $\tau$ . The full profile length must be entered as  $L$ , not the domain of ACF data which are often cut to a shorter  $\tau$  interval.

Expressions (27) and (28) differ only in coefficients of the bias terms, which are  $\sqrt{\pi}$  and 2 in the term linear in  $\alpha$  and 1 and 2 in the quadratic term. They are the same as in the corresponding polynomials for the bias of  $\sigma^2$  [1]. The linear term and quadratic term coefficients originate from

$$M_0[G] = \int_0^\infty G(u) du \quad \text{and} \quad M_1[G] = \int_0^\infty uG(u) du . \quad (29)$$

Other ACF models thus can be translated to the biased form

$$G^{\text{bias}}(\tau) = G(\tau) - 2n \frac{M_0[G]}{L} \left(1 + \frac{\tau}{L}\right) + 2n^2 \frac{M_1[G]}{L^2} \left(1 + \frac{2\tau}{L}\right) . \quad (30)$$

### 3.2. Model-free inversion

For an ACF of an unknown form, although still quickly monotonically decreasing, expressions (29)–(30) are written in the discrete form

$$\hat{G}_k = G_k^c - \frac{2n}{N} \left(1 + \frac{k}{N}\right) \sum_{m=0}^{K-1} G_m^c + \frac{2n^2}{N^2} \left(1 + \frac{2k}{N}\right) \sum_{m=0}^{K-1} mG_m^c \quad (31)$$

and solved as a set of  $K$  linear equations for corrected  $G_m^c$  with  $m = 0, 1, 2, \dots, K-1$ . Index  $K$  represents a cut-off after which the function is assumed to be negligible or the data not usable, i.e. again around the first zero crossing.

Although the equations could also be written in an explicitly matrix-like form

$$\sum_{m=0}^{K-1} R_{k,m} G_m^c = \hat{G}_k \quad (32)$$



with

$$R_{k,m} = \delta_{km} - \frac{2n}{N} \left(1 + \frac{k}{N}\right) + \frac{2n^2}{N^2} \left(1 + \frac{2k}{N}\right) m, \quad (33)$$

the form (31) shows that in this case the matrix multiplication, which would normally require  $\Omega(K^2)$  operations, reduces to two much simpler summations requiring only  $\Omega(K)$  operations because the sums

$$S_0[G^c] = \sum_{m=0}^{K-1} G_m^c \quad \text{and} \quad S_1[G^c] = \sum_{m=0}^{K-1} m G_m^c \quad (34)$$

do not depend on  $k$ . Therefore, they only have to be computed once:

$$\sum_{m=0}^{K-1} R_{k,m} G_m^c = G_k^c - \frac{2n}{N} \left(1 + \frac{k}{N}\right) S_0[G^c] + \frac{2n^2}{N^2} \left(1 + \frac{2k}{N}\right) S_1[G^c]. \quad (35)$$

The same holds for multiplication with  $R^T$  which simplifies to

$$\sum_{m=0}^{K-1} R_{k,m}^T G_m^c = G_k^c - \frac{2n}{N} \left(1 - \frac{kn}{N}\right) S_0[G^c] - \frac{2n}{N^2} \left(1 - \frac{2kn}{N}\right) S_1[G^c] \quad (36)$$

The linear system

$$R^T T G^c = R^T \hat{G} \quad (37)$$

has a positive definite matrix. Therefore, the method of conjugated gradients [13,14] can be used to solve it quickly as all matrix multiplications (35) and (36) are computationally cheap. Starting from the initial estimate  $G_k^c = \hat{G}_k$ , only a couple of iterations are required for convergence.

## 4. Numerical and experimental examples

### 4.1. Simulated data—Gaussian ACF

We first compare the performance of standard and biased Gaussian roughness models (5) and (27) using simulated data. Synthetic rough Gaussian surfaces were generated using the spectral method with  $T = 20$  px. The correlation length is in the typical range for real AFM images, regardless of the physical dimensions of the scanned area. The mean square roughness  $\sigma$  was set to 1 as it is only a scaling parameter. The image size varied from 100 px to 2000 px, corresponding to  $\alpha$  from 0.01 to 0.2 (in the reverse order). The discrete ACF (25) was evaluated using the standard Fast Fourier Transform method, after levelling image rows using polynomials with degrees from 0 to 2.

The polynomial levelling was, of course, not actually necessary here because the simulated data were ideal and had neither tilt nor bow. It simulated the effect of preprocessing that would be applied to measured data. Tilt or bow could be added beforehand, but it would be pointless. The levelling would subtract them again, together with a part of the roughness—which is the effect we are studying.

Marquardt–Levenberg algorithm was used for the non-linear least squares fitting to obtain  $\sigma$  and  $T$ . Both models were fitted to data up to the first zero crossing. The

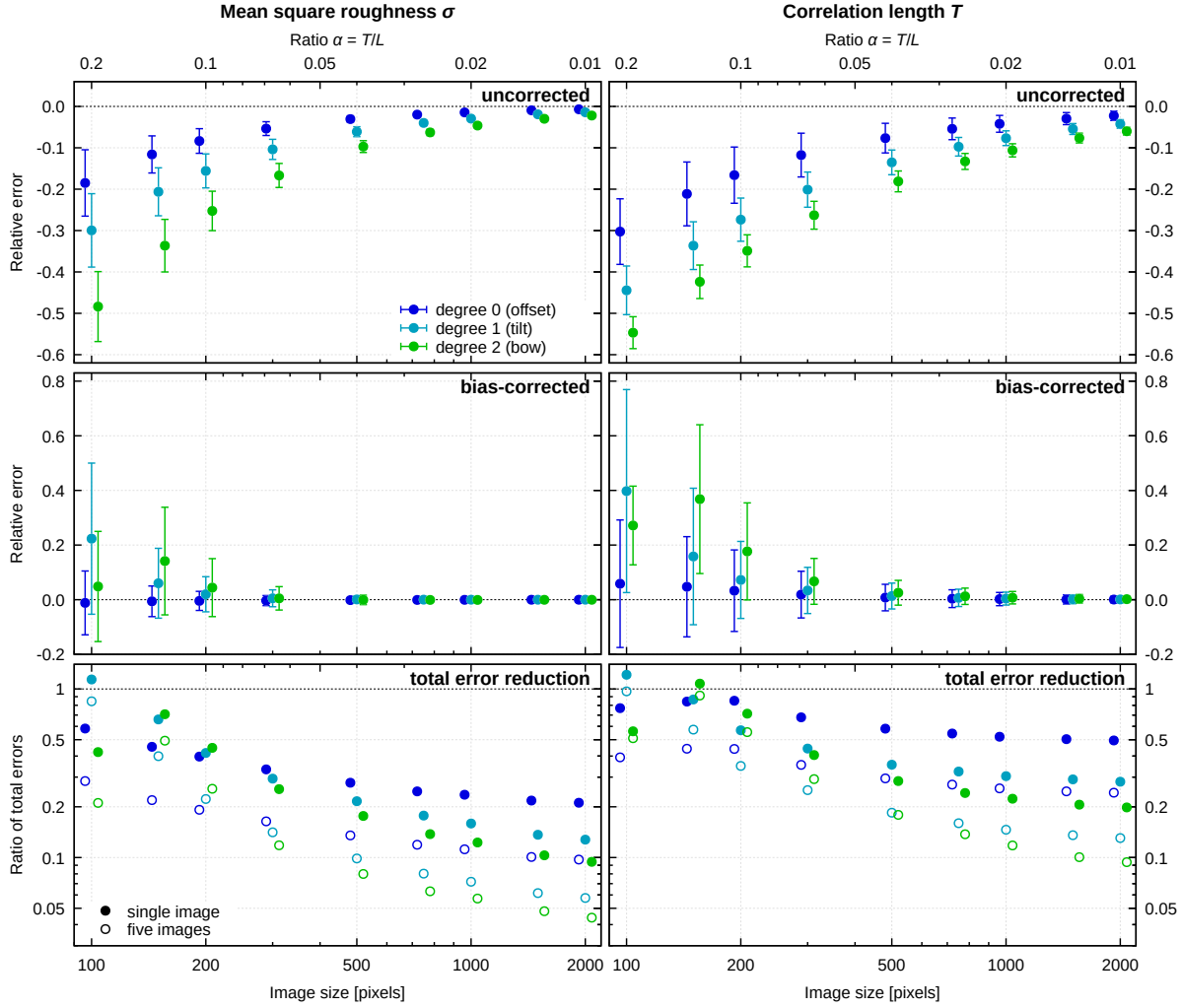


**Figure 3.** Comparison of fitting the biased Gaussian ACF model (27) with the standard one (5) (for correlation length of 20 px). Error bars represent single-image standard deviations. Results for different polynomial degrees are slightly offset horizontally for visual clarity.

entire procedure was repeated with randomly generated Gaussian surfaces hundreds of times (with more repetitions for smaller images for which the variances are larger). The means and standard deviations are plotted in figure 3.

The biased model (27) clearly succeeded at bias reduction. For both parameters and almost all image sizes the bias becomes so small that it is no longer an issue. The only exception is very small images which are only several correlation lengths large ( $\alpha \lesssim 1/10$ ). Although bias usually still decreases, it is at the cost of greatly increased variance. Too much roughness information is missing in such small areas. Using them for roughness evaluation is just wrong and the correction cannot change it.

The correction generally trades the bias for variance, i.e. the parameters have larger variances than for the standard model. For reasonable  $T/L$  the trade-off is advantageous. The total error ( $\text{variance} + \text{bias}^2$ )<sup>1/2</sup> decreases as illustrated in the bottom row of figure 3.

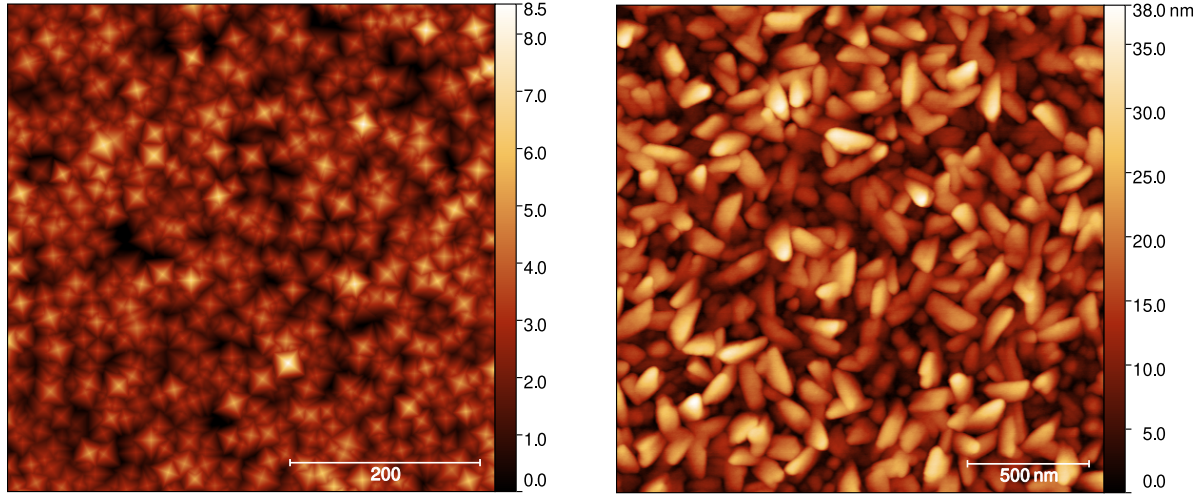


**Figure 4.** Small parts ( $512 \times 512$ ) of surfaces used in the model-free correction (inversion) examples. Left: simulated random pyramids. Right: polycrystalline SrO thin film.

The improvement is more marked for  $\sigma$  where it can be an order of magnitude, whereas for  $T$  it ranges from about  $2\times$  to  $5\times$ . The improvement is larger for higher polynomial degrees. The reason appears to be that the bias is larger in absolute value, but of the same functional form. Hence, the same correction is able to deal with a larger bias.

Full circles in figure 3 correspond to the worst case scenario of a single-image roughness measurement. Multiple scans reduce the variance, the dominant contribution for the improved model, but do not help with bias, the dominant contribution for the standard one. This is illustrated in the plot of total error reduction for five-image evaluation (open circles).

#### 4.2. Simulated data—inversion

For model-free correction (inversion) random pyramidal surfaces with an unknown ACF were generated using Gwyddion [15] *Objects* function which generates surfaces by sequential ‘extrusion’ [16]. The pyramids were randomly oriented and the pattern was large-scale isotropic. The generated images were  $8000 \times 8000$  pixels, corresponding to approximately 700 correlation lengths ( $\alpha \approx 0.0015$ ). A small ( $512 \times 512$ ) part of one such image is shown in figure 4. Smaller images of various sizes were again cut from the large base image and used to estimate the ACF.

The corrected ACF was computed by cutting  $\hat{G}_k$  slightly beyond the first zero crossing (10 % farther) and solving the linear system (31) as described in section 3.2. Roughness parameters  $\sigma$  and  $T$  were again evaluated from both the biased and corrected ACF. In particular  $\sigma$  was calculated from the relation  $\sigma^2 = G_0$  and  $T$  as the distance at which the ACF first falls to  $G_0/e$  ( $e$  being Euler’s number). The  $1/e \approx 0.368$  threshold is consistent with the analytic models (5) and (26), although it should be noted that roughness measurement standards often set the threshold differently, 0.2

being a common choice [17].

The comparison also requires true values of  $\sigma$  and  $T$ . They were obtained using angularly averaged 2D ACF, which was averaged over all generated images. The data were artificial and did not contain any tilt, bow, sample bending or other type of background. Therefore, the only preprocessing necessary before the computation of 2D ACF was the subtraction of the mean value from the entire image. The relative bias introduced by this operation is of the order of  $\alpha^2$  [1, 8], i.e.  $< 10^{-5}$  and thus negligible.

The results are plotted in figure 5. The overall trends are similar as for the modified Gaussian model fitting, but the accuracy improvements are more moderate. Although an improvement by factor of 2 is still not negligible, it is only observed for degree 2 levelling. For mean value subtraction the correction may not be worth the effort (at least with single-image evaluation) and can in fact even make the total error slightly larger. While  $\sigma$  is corrected almost perfectly,  $T$  appears slightly overcorrected, leaving a small bias and weakening the effectiveness, especially for large images where the error is already small. Multi-image evaluation (open circles) again increases the total error improvement.

We also tested how the correction depends on the ACF cut-off point by choosing the interval from 10% shorter to 40% longer than to the first zero crossing. The effect can be assessed using the accuracy of  $\sigma$  and  $T$  or differences between the corrected and true ACF curves. All the dependencies are generally quite flat and often without any clear trend. This is a reassuring result because it means the correction is not sensitive to the cut-off point precise location. As expected, for very tiny images (large  $\alpha$ ) shortening the interval improves the accuracy somewhat. For large images (small  $\alpha$ ) the trend was sometimes slightly opposite. Overall, however, cutting at the first zero crossing or moderately beyond it appeared to work well.

#### 4.3. Rough thin film—inversion

Ideally, a test with real rough surface would be done with a sample whose ACF is precisely known and can be used for reference. Due to the lack of such standard samples, the true—or best estimate—ACF has to be obtained in a manner similar to the previous section. An SrO thin film, prepared by atomic layer deposition, with large-scale uniformly and isotropically rough upper surface was chosen for the demonstration (see figure 4). Images were acquired using a Bruker Dimension Icon atomic force microscope in ScanAsyst mode with a standard ScanAsyst-air probe and scan rate of 0.2 Hz. In order to follow the 2D ACF route, a large image without scan line artefacts is necessary. The absence of scan line artefacts means 2D polynomial levelling is sufficient, leaving only bias proportional to  $\alpha^2$  (or higher powers). A scan of area  $12 \times 12 \mu\text{m}^2$  with pixel resolution of  $3072 \times 3072$  was selected for the evaluation. The correlation length to scan size ratio was estimated as  $\alpha \approx 0.0037$ , meaning the relative bias following from background subtraction was  $< 10^{-3}$ . The resulting ACF is plotted in figure 6 (each subplot) and separately also in figure 7.

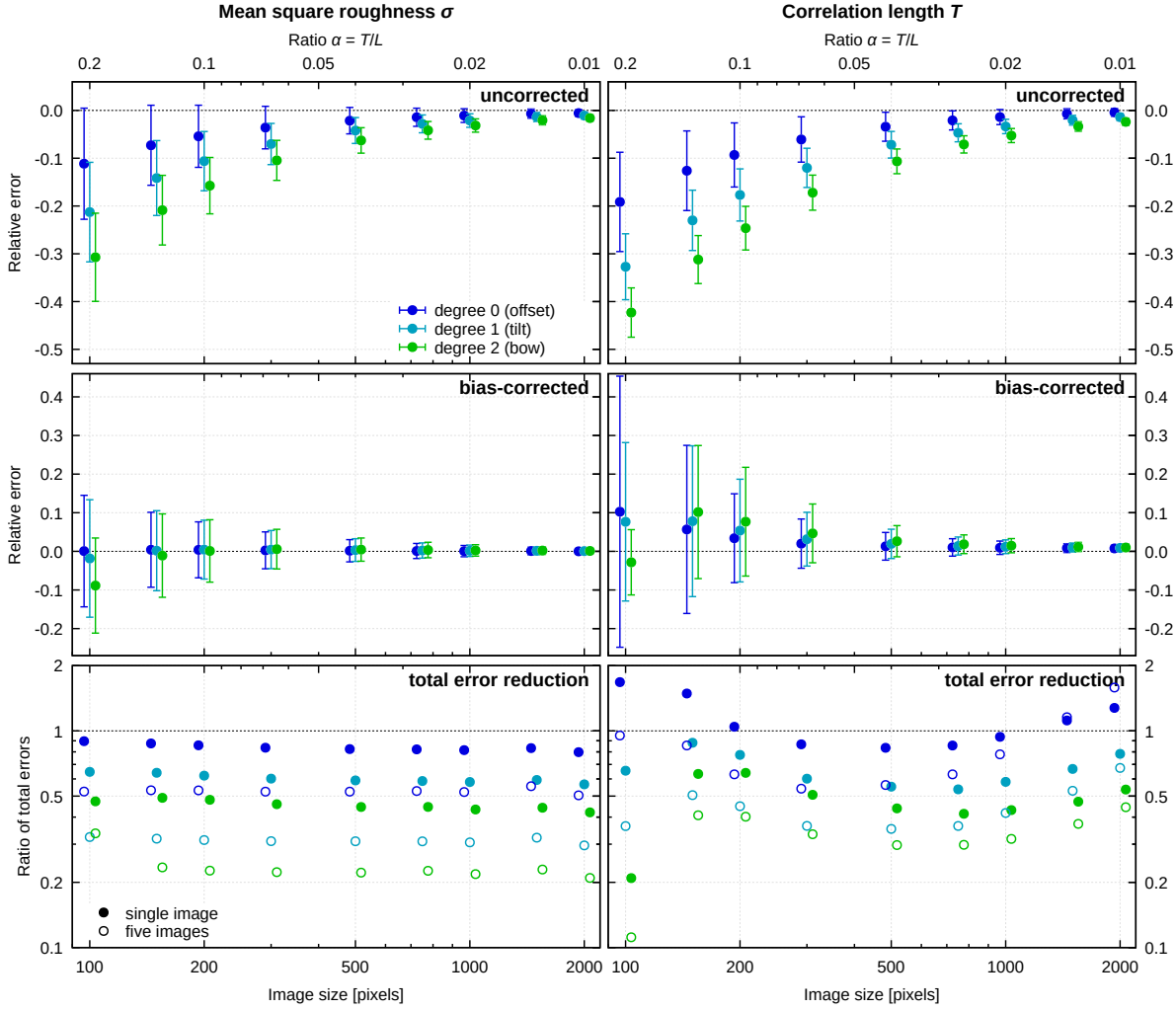


**Figure 5.** Comparison of roughness parameters  $\sigma$  and  $T$  obtained from uncorrected and model-free corrected ACF curves for a random pyramidal surface. Error bars represent single-image standard deviations. Results for different polynomial degrees are slightly offset horizontally for visual clarity.

The large image was then cut to smaller images of various sizes and processed as above, assuming subimages are reasonable approximations of measurements on smaller areas. The uncorrected (red) and corrected (green) ACF computed for each subimage are plotted in figure 6 for three selected sizes and all three polynomial degree 0–2. The corrected ACF curves were extrapolated beyond the cut-off points by a simple subtraction of the last computed correction from all further data (cyan).

The correction is clearly effective. The green (corrected) curves, although spread slightly more than the red (uncorrected), are centred on the best estimate ACF. Deviations are noticeable only for the highest degree and the far ends of the curves, where there is a tendency to overcorrection.

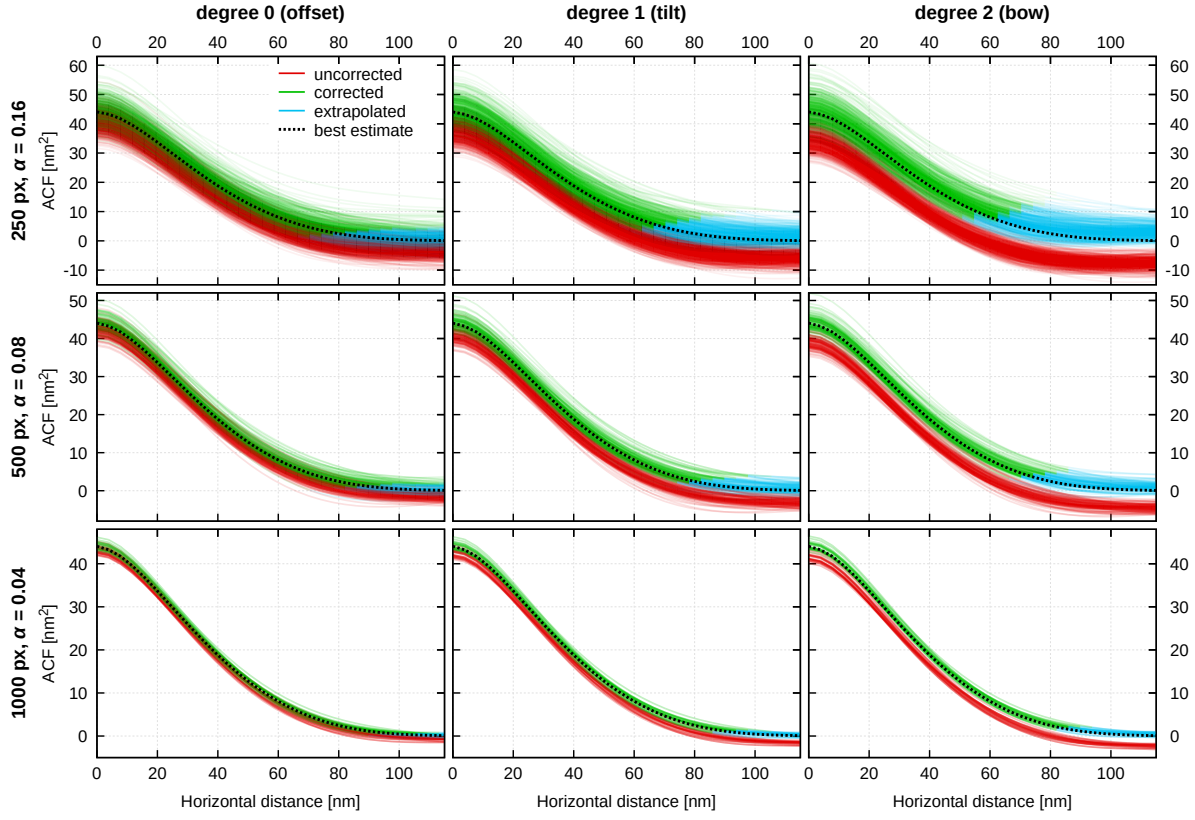


**Figure 6.** Autocorrelation functions obtained by model-free correction for rough SrO film surface, compared to uncorrected ACF and the best-estimate ACF. Each curve corresponds to one subimage cut from the large base image.

## 5. Discussion

We first remark on the normalisation factor in (25) which is sometimes taken to be  $1/N$  instead of  $1/(N - k)$  because of positive definiteness and/or variance [7, 18, 19]. It corresponds to dividing the integrals in section 2 by  $L$  instead of  $L - \tau$ . However, the estimator with  $N - k$  denominator is unbiased (without background subtraction) and the one with  $N$  does not generalise to irregular regions and other cases where varying amount of data is available for different distances  $\tau$  [15].

### 5.1. Interpretation of results

Figure 6 almost looks too good to be true. One has to be careful with its interpretation. Everything was computed from the same large base image. The clustering of the green curves around the best estimate shows that we removed the bias tied to smaller scan areas. However, they do not necessarily cluster around the *true* ACF. In the example with synthetic Gaussian and pyramidal data, the surfaces were uniform and could be made infinite for all practical purposes. But for real rough surfaces, the issues of uniformity, representativeness and the statistical character of roughness are much more tangled. It should also be noted that roughness measurement is also affected by

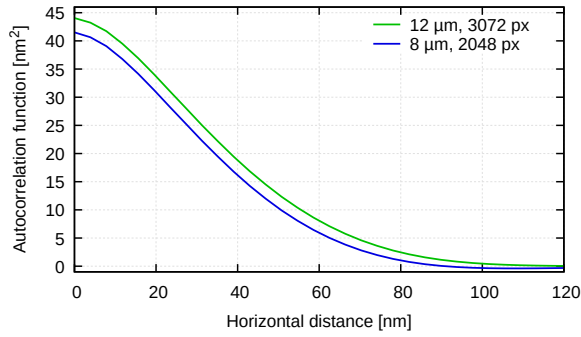


**Figure 7.** Comparison of best-estimate ACF obtained using independent scans of two different areas.

tip sharpness and probe-sample interaction in general [20–23], sampling step [21, 24], calibration, scanning speed and feedback loop settings [22], defects, and other effects not analysed here as we attempt to isolate those related to the finite area.

The measurement of a neighbour region (slightly smaller,  $8 \times 8 \mu\text{m}^2$ ) results in a different ACF, as illustrated in figure 7. Subimages taken from this scan yield curves centred on its own best-estimate ACF. The bias estimates for the two images are approximately  $3 \times 10^{-4}$  and  $6 \times 10^{-4}$ . The relative standard deviations of  $G(0) = \sigma^2$  are proportional to  $\alpha$  [8] were estimated as  $2 \times 10^{-3}$  and  $3 \times 10^{-3}$ . They are all too small to explain the difference of almost 6% between the two curves. The correlation length does not capture the scale at which real textures can be considered uniform. Although surface heights become uncorrelated for points considerably farther apart than  $T$ , the texture itself varies along the surface. The characteristic scale of these variations can be much longer than  $T$  even if the texture is ultimately large-scale uniform. Scanning such large areas is seldom feasible and we have to rely on multiple independent scans.

## 5.2. Comparison with spectral density

Two other functions are commonly used to characterise spatial properties of roughness, height-height correlation function [8] (sometimes also called structure function) and power spectrum density function (PSDF). Height-height correlation function  $H$  is directly related to ACF by  $H(\tau) + 2G(\tau) = 2\sigma^2$ , so the results can be translated. PSDF is the Fourier transform of ACF and is probably the most commonly utilised function [21, 25]. The effect of levelling is suppression of low-frequency components [2].

The low-frequency components can be excluded from fitting, similarly how the ends of spectral range are avoided in PSDF stitching [18, 21, 26–28]. However, the peak around zero frequency is where almost all the spectral weight lies. It is also the least affected by noise, discontinuities and smoothing effects such as tip convolution [21, 22, 25]. It is often critical in roughness analysis. However, it is the region worst affected by levelling, and possibly in a non-trivial manner. In the case of ACF the worst affected region is far from the origin and it is never used for analysis. Around the origin, levelling manifests as the



subtraction of a slowly varying function. An approach similar to the one developed here can perhaps be formulated also for PSDF—Ref. 1, for instance, gives hints at spectral reinterpretation. However, what would be the equivalent of model-free correction for PSDF is not clear.

### 5.3. Zero crossing

The model-free correction procedure relies on the true ACF monotonically and quickly decaying to zero. In particular, expressions (34) must give good approximations of integrals (29) (or similar integrals, but up to  $L$  instead of infinity). Even though it is true for many types of real roughness, at least approximately, some violate this condition. For instance if the surface is locally periodic/corrugated the true ACF crosses zero, possibly many times. It may be possible to modify the correction procedure for this case, but likely at the cost of reliability. And although the approach of fitting  $\hat{G}_k$  with biased model remains intact in principle, the choice of fitting cut-off becomes more complicated.

All the procedures also utilise the zero crossing for choosing the cut-off. Must there always be a zero crossing? By splitting the sum  $z_m z_k$  over all  $m$  and  $k$  into triangular parts and correcting for the double-counted diagonal

$$\sum_{m,k=0}^{N-1} z_m z_k = 2 \sum_{k=0}^{N-1} \sum_{m=0}^{N-1-k} z_{m+k} z_k - \sum_{k=0}^{N-1} z_k^2 = 2 \sum_{k=0}^{N-1} (N-k) \hat{G}_k - N \hat{G}_0. \quad (38)$$

The left hand side is zero since the mean value of  $z$  is zero. Therefore,

$$-\frac{N}{2} \hat{G}_0 + \sum_{k=0}^{N-1} (N-k) \hat{G}_k = \frac{N}{2} \hat{G}_0 + \sum_{k=1}^{N-1} (N-k) \hat{G}_k = 0 \quad (39)$$

and  $\hat{G}_k$  must take both signs. As for the crossing location, the leading term approximation of (30) or (31) is a small constant (proportional to  $M_0[G]$  or  $S_0[G]$ ). If ACF decays quickly, the first zero crossing occurs when the true ACF is equal to this constant. And this is also when  $S_0[G]$  and  $S_1[G]$  can be assumed to give good approximations to the corresponding integrals.

For biased model fitting, the heuristic zero-crossing rule is further supported by the following:

- The rule is simple and easy to implement both manually and in code.
- Fitting only data of the apex at origin is an ill-conditioned problem. The optimal bias–variance trade-off invariably includes the side slopes in the fit. Shortening the interval too much cannot be beneficial.
- Although fitting beyond the zero crossing may be beneficial, often the ACF is not converged in this region and telling where useful data end is difficult.
- Numerical simulations support the zero crossing as a good choice (section 4.2).



## 6. Conclusion

The goal of this work was to correct the finite-area bias in autocorrelation function (ACF) evaluation in roughness measurements, which includes the correction of parameters like the mean square roughness and correlation length. Starting from the observation that it should be possible to express the bias of measured ACF in terms of ACF itself, we developed a self-consistent formulation and used it to propose two types of bias correction. One was a modification of standard ACF models to match the bias of the data they should fit, the other a model-free correction procedure based on inverting the self-consistent relations by solving a set of linear equations. Their effectiveness was tested using simulated and measured data. The results were somewhat mixed. Both corrections trade bias for variance. In some cases, such as the measurement of Gaussian roughness, fitting the experimental ACF with a modified (biased) model has substantial advantages and few downsides and can probably be recommended quite universally. Model correction does not require any changes to ACF estimation and can be applied to already computed ACF curves. A corrected model can be easily constructed for any quickly decaying ACF. Its effectiveness can vary as it depends on the ACF form and other aspects of the measurement. Scan line levelling with polynomials of higher degrees than 0 (i.e. mere mean value subtraction) and measurement using multiple images make the correction more advantageous. The model-free correction (inversion) procedure proposed for ACF of an unknown form is computationally simple and worked surprisingly well in the selected test cases. However, reliability and applicability questions remain and it is perhaps more of an interesting concept to explore further than a technique which could be recommended for immediate wide adoption.

## Acknowledgements

I would like to thank my colleagues Marek Eliáš and Lenka Zajíčková for the rough samples used in the experimental part. TheCzechNanoLab project LM2023051 funded by MEYS CR is acknowledged for the financial support of the measurements and sample fabrication at CEITEC Nano Research Infrastructure.

## References

- [1] Nečas D, Klapetek P and Valtr M 2020 *Meas. Sci. Technol.* **31** 094010
- [2] Nečas D, Valtr M and Klapetek P 2020 *Sci. Rep.* **10** 15294
- [3] Starink J P and Jovin T M 1996 *Surface Science* **359** 291–305
- [4] Erickson B W, Coquoz S, Adams J D, Burns D J and Fantner G E 2012 *Beilstein J. Nanotechnol.* **3** 747–758
- [5] Wang Y, Lu T, Li X and Wang H 2018 *Beilstein J. Nanotechnol.* **9** 975–985 ISSN 2190-4286
- [6] Marinello F, Bariani P, Chiffre L D and Savio E 2007 *Meas. Sci. Technol.* **18** 689
- [7] Anderson T W 1971 *The Statistical Analysis of Time Series* Wiley series in probability and mathematical statistics (New York: John Wiley & Sons)
- [8] Zhao Y, Wang G C and Lu T M 2000 *Characterization of Amorphous and Crystalline Rough*

*Surface – Principles and Applications (Experimental Methods in the Physical Sciences vol 37)*  
(San Diego: Academic Press)

- [9] Krishnan V and Chandra K 2015 *Probability and Random Processes* 2nd ed (Wiley)
- [10] Hyndman R and Wand M 1997 *Australian Journal of Statistics* **39** 313–324
- [11] Park C, Hannig J and Kang K H 2009 *Statistica Sinica* **19** 1511–1530
- [12] Maxima 2023 Maxima, a computer algebra system. version 5.45.1 URL <https://maxima.sourceforge.io/>
- [13] Hestenes M R and Stiefel E 1952 *J. Res. Nat. Bur. Stand.* **49** 409–436
- [14] Golub G H and Meurant G 2010 *Matrices, Moments and Quadrature with Applications* (New Jersey: Princeton University Press)
- [15] Nečas D and Klapetek P 2012 *Cent. Eur. J. Phys.* **10** 181–188
- [16] Nečas D and Klapetek P 2021 *Nanomaterials* **11** 1746
- [17] ISO 25178 2012 Geometric product specifications (GPS) – surface texture: Areal
- [18] Panda S, Panzade A, Sarangi M and Roy Chowdhury S K 2016 *Journal of Tribology* **139** 031402
- [19] Bittani S 2019 *Model Identification and Data Analysis* (Agawam: Wiley)
- [20] Sedin D L and Rowlen K L 2001 *Appl. Surf. Sci.* **182** 40–48 ISSN 0169-4332
- [21] Jacobs T D, Junge T and Pastewka L 2017 *Surface Topography: Metrology and Properties* **5** 013001
- [22] González Martínez J F, Nieto-Carvajal I, Abad J and Jaime C 2012 *Nano Express* **7** 174
- [23] Leach R, Weckenmann A, Coupland J and Hartmann W 2014 *Surface Topography: Metrology and Properties* **2** 035001
- [24] Sanner A, Nöhring W G, Thimons L A, Jacobs T D and Pastewka L 2022 *Applied Surface Science Advances* **7** 100190
- [25] Rutigliani V, Lorusso G F, Simone D D, Lazzarino F, Rispens G, Papavieros G, Gogolides E, Constantoudis V and Mack C A 2018 Setting up a proper power spectral density (PSD) and autocorrelation analysis for material and process characterization *Metrology, Inspection, and Process Control for Microlithography XXXII (Proc. SPIE vol 10585)* ed Ukraintsev V A and Adan O p 105851K
- [26] Duparre A, Ferre-Borrull J, Gliach S, Notni G, Steinert J and Bennett J 2002 *Appl. Opt.* **41** 154–171
- [27] Gong Y, Misture S T, Gao P and Mellott N P 2016 *The Journal of Physical Chemistry C* **120** 22358–22364
- [28] Klapetek P, Yacoot A, Grolich P, Valtr M and Nečas D 2017 *Meas. Sci. Technol.* **28** 034015